



High-rate cathode CrSSe based on anion reactions for lithium ion battery

Journal:	<i>Journal of Materials Chemistry A</i>
Manuscript ID	TA-ART-08-2020-008012.R2
Article Type:	Paper
Date Submitted by the Author:	15-Oct-2020
Complete List of Authors:	<p>Yang, Si-Yu; Fudan University Department of Chemistry Shi, Ding-Ren; Fudan University Department of Chemistry Wang, Tian; Fudan University Department of Chemistry Yue, Xin-Yang; Fudan University, Department of Materials Science Zheng, Lei; Institute of High Energy Physics, Chinese Academy of Sciences, Beijing Synchrotron Radiation Facility Zhang, Qing-Hua; Chinese Academy of Sciences Gu, Lin; Institute of Physics Chinese Academy of Sciences, Beijing Laboratory of Electron Microscopy Yang, Xiao-Qing; Brookhaven National Lab, Chemistry Shadike, Zulipiya; Brookhaven National Laboratory, chemistry division Li, Hong; Institute of Physics, Chinese Academy of Sciences, Fu, Zhengwen; Department of Chemistry,</p>

ARTICLE

High-rate cathode CrSSe based on anion reactions for lithium ion battery

Received 00th January 20xx,
Accepted 00th January 20xx

Si-Yu Yang,^{#a} Ding-Ren Shi,^{#a} Tian Wang,^a Xin-Yang Yue,^b Lei Zheng,^c Qing-Hua Zhang,^d Lin Gu,^d Xiao-Qing Yang,^e Zulipiya Shadike,^{*e} Hong Li,^{*fg} Zheng-Wen Fu^{*a}

DOI: 10.1039/x0xx00000x

Studies of transition metal dichalcogenides (TMDs) can be traced back to the 1970s but have been abandoned for a while due to the fire hazard of lithium metal batteries. Herein, a new layered material CrSSe is reported, whose intercalative capacity can achieve 190 mAh g⁻¹ with charges all compensated by anionic S and Se. Fascinating performances of half-cell have also been presented, with a capacity retention rate of 81.5% upon 1000 cycles at 20C and high putout of 101.7 mAh g⁻¹ even at 200C. In addition, an ideal way to build a type of full battery without lithium anode for CrSSe is also displayed with the Li₃N film was synthesized on the electrode surface as lithium source. Overall, discovery of CrSSe enriches the chemistry of TMDs and the application in full batteries opens opportunities for enabling the lithium-free cathodes to be widely utilized in practical.

Introduction

Early studies on lithium intercalation in layered electrode material dichalcogenides transition metal dichalcogenides (TMDs) have led to the development of rechargeable lithium battery, in which TiS₂ cathode was firstly constructed by Exxon in the 1970s.¹ Then MoS₂ was investigated as a intercalative cathode in lithium metal batteries after a dozen years.² However, safety issues arising from dendritic lithium growth and flammability of the organic electrolyte lead to discontinuation of battery with lithium anode. From then on, lithium contained layered oxides materials such as LiCoO₂, LiNi_{1-y}Co_yO₂, and LiNi_xMn_yCo_{1-x-y}O₂ obtaining the same layered structures with LiTiS₂, namely the discharged state of TiS₂, as their relays lead the new era of battery cathode materials.³ Recently, the oxygen anionic redox reaction in Li-rich layered cathode materials becomes the center of attention due to their high energy density. Thus, it is very challenging to find new

layered materials based on anion reaction for enriching the intercalation chemistry and their potential applications in LIBs.

Layered disulfides have been considered as attractive candidates for cathode materials of high-power lithium batteries thanks to their favorable intercalation kinetics and high energy density.⁴⁻⁹ Titanium disulfide as the most classic one exhibited a typical single-phase (solid-solution) reaction with reversible cationic (Ti⁴⁺/Ti³⁺) redox over the entire range of the reaction, 0 ≤ x ≤ 1, in Li_xTiS₂.^{4, 5} VS₂ with similar structural evolution upon Li (de)intercalation experienced higher reduction potential of the V⁴⁺/V³⁺ couples for higher energy densities.^{6, 7} Based on the order of reduction potentials of Ti⁴⁺/Ti³⁺ < V⁴⁺/V³⁺ < Cr⁴⁺/Cr³⁺, CrS₂ may be more desirable for high-energy density batteries as a cathode, but has not been reported yet because of the instability.⁸ Interestingly, CrSe₂ has been successfully synthesized and investigated.¹⁰ Here, CrSSe was synthesized for the first time, in which the band of Cr-3d lies below S-3p and Se-4p so that charge compensation from S and Se has been permitted and the anionic redox reaction has been realized.

To further promote its application in LIBs, Li₃N film has been introduced to provide the lithium source needed for lithium-ion migration between CrSSe cathode and soft carbon anode, which is employed by depositing metal lithium film on the electrode surface and then in situ being nitridated. Our results have demonstrated that, new types of batteries with high-rate layered cathode CrSSe, which based on anion reaction, have been successfully realized.

Results and discussion

^a Shanghai Key Laboratory of Molecular Catalysts and Innovative Materials, Department of Chemistry, Fudan University, Shanghai, 200433, China.

^b Beijing Key Laboratory of Green Chemical Reaction Engineering and Technology, Department of Chemical Engineering, Tsinghua University, Beijing, 100084 P.R. China

^c Institute of High Energy Physics, Chinese Academy of Sciences, 19B Yuquan

^d Beijing National Laboratory for Condensed Matter Physics, Institute of Physics, Chinese Academy of Sciences, PO Box 603, Beijing 100190, P.R. China.

^e Chemistry Division, Brookhaven National Laboratory, Upton, NY, 11973 USA

^f Tianmu Lake Institute of Advanced Energy Storage Technologies, Yangtze River Delta Physics Research Center, Liyang City, Jiangsu, 213300, China

^g Institute of Physics, Chinese Academy of Sciences, Beijing, 100190, China

[#] These authors contributed equally: Si-Yu Yang and Ding-Ren Shi

*Corresponding authors

Electronic Supplementary Information (ESI) available: [SEM image, STEM image, Raman spectrum, Cr K-edge XANES spectrum and Se K-edge FT-EXAFS spectrum of CrSSe. Partial density of states of S-3p and Se-4p for CrSSe and LiCrSSe. Charge-discharge curves and cycling performances for half cells of CrSSe-Li₃N/Li and SC-Li₃N/Li.]. See DOI: 10.1039/x0xx00000x

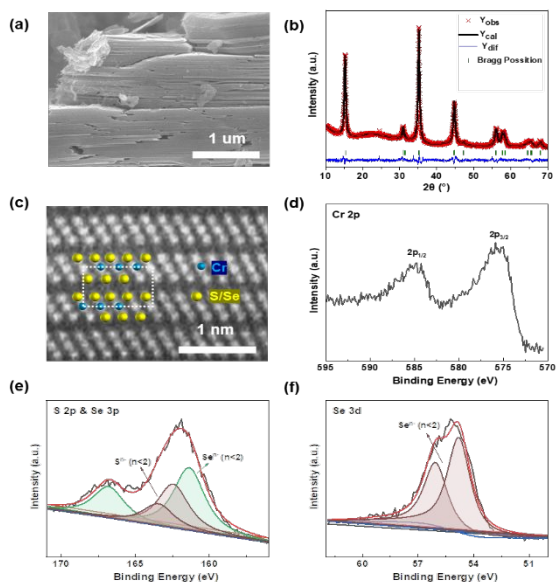


Figure 1. (a) SEM images, (b) the refinement of XRD pattern and (c) STEM images of CrSSe; (d) Cr 2p, (e) S 2p & Se 3p and (f) Se 3d XPS results of CrSSe.

Physical, chemical and electrochemical properties of CrSSe

CrSSe was prepared via chemical deintercalation method by oxidizing NaCrSSe with iodine, which has also been used regarding the synthesis of CrSe₂ but failed for CrS₂.¹⁰ The obtained product is a sort of greyish-black powder and scanning electron microscope (SEM) image reveals that it possesses a shape of close-stacked platelets with a thickness range of 60 nm or so (Figure 1a and Figure S1). The Rietveld refinement result of X-ray diffraction (XRD) pattern of CrSSe sample is shown in Figure 1b and Table S1, in which the low value of R ($R_{wp} = 1.79\%$, $R_p = 1.37\%$) stands for the excellence of fit. High crystallinity is also presented, additionally, the Bragg reflections all belong to the space group P-3m1 without obvious impurities, showing the similarity with the structure of CrSe₂.¹¹ Three main peaks located at 15.2°, 35.2° and 44.7° can be assigned to the crystal planes of (001), (101) and (102) respectively, and the preferred orientation of (001) is indicative to the two-dimensional (2D) nature of nanoflakes. Table S1 lists the lattice parameters of refinement, in which the interlayer spacing ($c = 5.78 \text{ \AA}$) is about 2.43% lower than that of CrSe₂ by replacing half amount of selenium atoms with sulfur, leading to a higher energy density of battery served as electrode.

The scanning transmission electron microscopy (STEM) image in Figure 1c and Figure S2 further displays that atoms are arranged in perfect order of O1-type stacking without any area falling into disarray, which may lead to the formation of dimers. Considered that Raman spectroscopy is sensible to detect pairs of S-S, S-Se, and Se-Se dimers over the range of 150-600 cm⁻², none of the information can be seen in Figure S3 gives direct proof that no dimerization happens during the

synthesis of CrSSe. Analysis of chemical components was then conducted via measurements of X-ray photoelectron spectroscopy (XPS) and ion-beam cleaning was done at first to remove the surface contaminations. As shown in Figure 1d, the high-resolution spectrum of Cr 2p presents single doublet at 584.9/575.6 eV, alluding to the trivalent state of chromium.¹² Besides that, peaks centered at 162.5 and 163.5 eV in Figure 1e should be identified as the S species with core-hole effects (S^{n-} , $n < 2$).¹³ And pairs of Se 3p (Figure 1e) and Se 3d (Figure 1f) at binding energies of 161.4/166.8 eV and 54.8/56.1 eV demonstrate the presence of Se^{n-} ($n < 2$).¹⁴

Next, Li-storage properties of CrSSe were probed in half-cell with metal lithium as the anode and Figure 2a shows the charge/discharge curve obtained at 1C (1C=164 mAh g⁻¹). Intercalation of exactly one molar lithium ion can be achieved when discharging to 1.5 V. Moreover, no other plateau occurs until 1.0 V while deeper lithiation can be realized with a reversible capacity of about 190 mAh g⁻¹. Then the conversion reaction happens as continuously when decreasing the cutoff voltage, with the discharge capacity reaches to 350 and 595 mAh g⁻¹ or so when reaching 0.9 V and 0.6 V, respectively (Figure 2b). XRD patterns of fully recharged electrodes further demonstrate that (001) reflection of CrSSe at 15.2° can be discerned even if the cell discharging to 0.9 V, indicating the layered structure of material is still preserved even if the conversion reaction has happened at this point. However, none of the crystalline information can be seen as the discharge cutoff voltage is down to 0.6 V, which means the structure of CrSSe was totally collapsed after the conversion reaction taking place in this degree (Figure 2c). Cycling

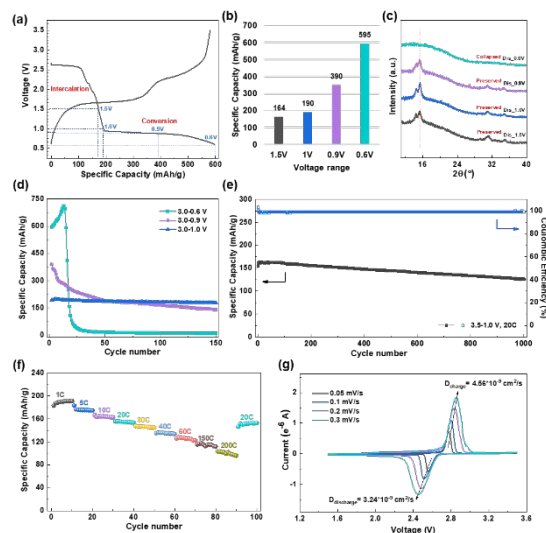


Figure 2. (a) Charge-discharge curves of CrSSe within 3.5-0.6 V at 1C; (b) initial discharged capacity, (c) XRD patterns of recharged electrodes and (d) cycle performance at 1C for different voltage ranges; (e) long-term cycle performance at 20C in 3.5-1.0 V, (f) rate performance in 3.5-1.0 V and (g) CV profile in 3.5-1.5 V. All the electrochemical tests were performed at room temperature.

performance of the half-cell in various voltage windows at 1C is then evaluated and shown in Figure 2d, where CrSSe can stably cycle between 3.5 and 1.0 V, with a capacity of 176.9 mAh g⁻¹ after 150 cycles and retention rate of 91.8%. While in the voltage window of 3.5-0.9 V, though the initial capacity is up to 596.3 mAh g⁻¹, it undergoes a rapid decay right after that and the 150th capacity only remains at 140.7 mAh g⁻¹. Partial conversion reaction leads to the slight pulverization of active material and the happening of much more parasitic reactions with electrolyte, that's why the cyclic stability has been penalized to some extent.¹⁵ Several strategies such as element doping, surface coating and modification approaches should be studied to optimize the electrode surficial structure for the improvement of electrochemical performance in terms of cyclic stability in the future work. As the cell cycling within 3.5-0.6 V, the destruction of crystal structure brings about dramatic nanosizing of CrSSe particles, whose surface areas being exposed bigger and bigger, making the conversion reaction occur more and more thoroughly until be irreversible. Consequently, the capacity raises unexpectedly in the first 13 cycles but suddenly loses all its capacity afterwards. Based on the above analysis, 3.5-1.0 V is the optimum cutoff voltage range, within which both a relative high capacity delivery and a steady performance can be ensured. Following investigation in Figure 2e demonstrates that remarkable long-term cyclability can be realized even at 20C between 3.5 and 1.0 V, for 81.5% of the cell capacity still retains at the end of 1000 cycles with nearly unchanged coulombic efficiency of 100% during the overall process. The brilliant rate capability is also presented in Figure 2f, in which the capacity output of 190.4, 175.3, 164.3, 155.0, 146.5, 135.3, 126.3, 114.7 and 101.7 mAh g⁻¹ at 1, 5, 10, 20, 30, 40, 60, 150 and 200C, was achieved for lithium storage respectively. And it can recover to 151.7 mAh g⁻¹ as soon as the rate has been cut down to 20C.

Cyclic voltammetry (CV) measurements were also performed for studying the intercalation process (Figure 2g). A pair of symmetric peaks with undeformed shape can be detected at different scan rates, providing the evidence of a highly reversible electrochemical process. The anodic/cathodic peaks settle at 2.78/2.56 V when recorded at 0.05 mV s⁻¹ while shift to 2.85/2.45 V at 0.3 mV s⁻¹. For there has no significant Cr³⁺/Cr²⁺ redox couple at 2.1/1.9 V^{16,17}, the response over this potential range should be correlated to the redox reaction of S/Se in LIBs. In addition, the peak current (*i_p*) increases accompanied by the raising of scan rate (*v*) and *i_p* presents a linear dependence on *v*^{1/2} perfectly (Figure S4). According to the slope of the function, the diffusion coefficient (*D*) can be calculated to be 4.56 * 10⁻⁹ and 3.24 * 10⁻⁹ cm² s⁻¹ for the lithation and delithiation process, respectively. For the particle size of CrSSe is close to be 6 μm, it will just need 90 s for Li⁺ to migrate, simply estimated according to the relationship between diffusion length and time *L*²=*Dt*.¹⁸ In other words, theoretical capacity can still be achieved even at 40 C by

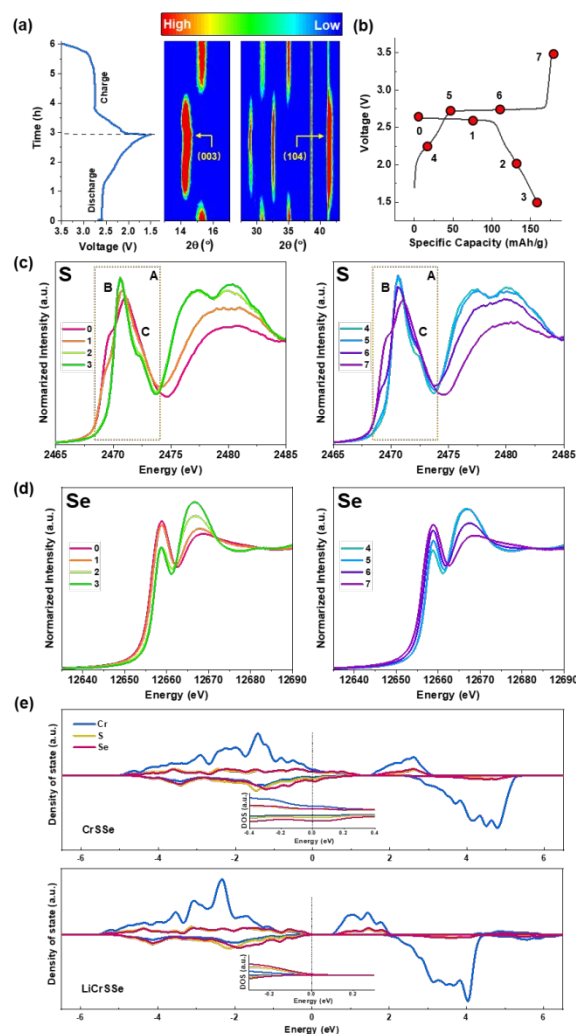


Figure 3. (a) In-situ XRD contour of CrSSe; (b) curves of the first cycle and the corresponding charge states at which data of ex-situ XAS have been recorded in sequence; XANES spectra at (c) S and (d) Se K-edges; (e) DOSs of CrSSe and LiCrSSe with the Fermi level marked by perpendicular lines.

calculation, though it has not been realized in practical due to the low electron conductivity between active particles. As an aside, the activation energy of Li⁺ hopping in Li_xCrSSe (0 < x ≤ 1) is found to be as low as 0.173 eV (when x = 0.5) compared with 0.4 eV for TiS₂ by simulation (Figure S5).¹⁹ The feature of 2D layered structure for CrSSe gives rise to the high value of diffusion coefficient and low diffusion barrier, which should be liable for the superior kinetic properties of the electrode as well as excellent cyclic and rate performance of the cell.

Structural evolution and charge compensation upon electrochemical cycling

As depicted in the contour maps (Figure 3a), the structural evolution of CrSSe was tracked by in-situ XRD on the initial discharge and charge. The pristine CrSSe is a typical layered material of O1 phase with (001) at 15.2° and (101) at 35.2° as main peaks. Apparently, the total removing of native Bragg reflections and emerging of new ones indicates that a

complete two-phase reaction is involved when embedding lithium ions. The fresh peaks with high intensities at 14.2° and 41.4° can be respectively regarded as crystal planes (003) and (104), or rather a new phase of O3 is formed for the newly generated compound LiCrSSe with an expansion of distance between two S/Se-Cr-S/Se slabs ($c/3 = 6.21 \text{ \AA}$). It is also worthy to notice that the structure of LiCrSSe is stably preserved upon discharging to 1.5 V, implying that only the conduct of intercalation happens to host in this potential range without any decomposition. During the recharge process, the peak evolution is exactly in the opposite way to the discharge one, representing the reversible behavior of phase transformation between CrSSe and LiCrSSe .

Subsequently, ex-situ x-ray absorption spectroscopy (XAS) was carried out for respective elements Cr, S and Se to figure out the variation of valence states in the electrochemical reactions. The spectrum of Cr K-edge X-ray absorption near-edge structure (XANES) and the corresponding Fourier transformed extended X-ray absorption fine structure (FT-EXAFS) are shown in Figure S6. Negligible changes of K-edge position at about 5996 eV can be observed for discharged and charged samples in Figure S6a, which all bears resemblance to the feature of NaCrS_2 , a clear indication of limited participation for Cr ions in the whole procedure of cycling. And slight shift for the bond lengths of Cr-S/Se and Cr-Cr in FT-EXAFS spectrum (Figure S6b and Table S2) confirms the limited valence change of Cr. In spite of this, the different line shape in pre-edge region upon the lithiation process of CrSSe should be related to the variation of Cr-Cr₆ hexagonal symmetry, for the intensity of bond Cr-Cr in FT-EXAFS spectrum has obviously increased.

20-22

For the sake of checking the redox degree of S and Se in detail, datasets of K-edge XANES at seven states of charge (Figure 3b) were collected. A hump (enclosed by yellow square and denoted as A) is embedded in the spectrum of S, whose area varies systematically in pace with the sequence of charge states (Figure S7). The damping of hump area upon lithiation is a character of depletion in numbers for the underfilled states of sulfur above the Fermi level. As observed more precisely in Figure 3c, the hump A consists of a weak pre-edge at 2469.8 eV and intense edge jump measured to be 2471.0 eV. The pre-edge peak, distinguished as S^{n-} ($n < 2$), undergoes a substantial drop of intensity and moves to 2469.0 eV at discharged state, which is suggestive of the depletion of electron holes and reduction of S ions.^{21, 23} While the broad edge can be split into two peaks, which has been clearly recognized upon discharging. One shifts toward a lower energy of 2470.6 eV (denoted as B) and the other (denoted as C) still at 2472.2 eV decreases in amplitude, ascribed to two bands of admixed S-3p/Cr-3d states,^{22, 24} which is a confirmation for S ions taking part in the reductive reactions. Also, the complete overlap of line shapes between the recharged and pristine states

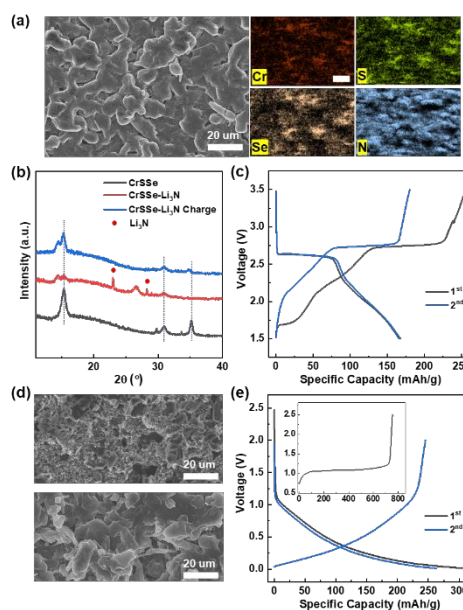


Figure 4. (a) SEM image and EDS mappings (scale bar: 20 μm) corresponding to element Cr, S, Se and N for $\text{CrSSe-Li}_3\text{N}$ electrode; (b) XRD patterns of electrode CrSSe , $\text{CrSSe-Li}_3\text{N}$ and $\text{CrSSe-Li}_3\text{N}$ after first charge; (c) charge-discharge curves for $\text{CrSSe-Li}_3\text{N/Li}$ half-cell; (d) SEM images for pristine soft carbon electrode (up) and $\text{SC-Li}_3\text{N}$ (down); (e) charge-discharge curves for $\text{SC-Li}_3\text{N/Li}$ half-cell.

confirms the reversibility of redox reaction for element sulfur.

Likewise, valence evolution can be monitored in the spectrum of Se (Figure 3d). The observation of sharp peak shrinking at 12658.9 eV, assigned to the dipole allowed transition from $1s$ to $4p$,^{25, 26} is a direct illustration of the decreased density of unoccupied Se-4p states in the vicinity of Fermi level when charge being compensated. Moreover, the shift of bump at ~ 12667 eV, determined by the multiple scattering of photoelectron in the neighboring p and d -like states,^{25, 26} owing to the change of chemical environment around Se atoms upon lithium uptake, which can be additionally certified by the Fourier-transformed extended X-ray absorption fine structure (FT-EXAFS) of Figure S8. The peak raised at 2.37 \AA , corresponding to the distance of Cr-Se bond allowing for the phase correction, which is reasonable to be a little smaller than the bond length in CrSe_2 .²⁷ It becomes slightly bigger to 2.42 \AA at the full state of discharge, indicating the valence state change of Se. All the above changes, both the resonances of XANES and EXAFS can be recovered closing to the pristine state through deintercalation, providing strong evidences for the reversible redox reactions of selenium.

Figure 3e is the density of states (DOSs) of Cr, S and Se in CrSSe and LiCrSSe computed by density functional theory (DFT) method to obtain the changing of electronic structure upon (de)lithiation. The significant overlap of three bands in CrSSe , which are respectively dominated by Cr-3d, S-3p and Se-4p, shows strong hybridization between Cr and S/Se orbitals. And

a kind of metallic behavior has been revealed, for bands all spread across the Fermi level (E_f), mainly due to the involvement of Se in system of TMDs.²⁸ While in the spectrum of LiCrSSe, no unoccupied electronic states at the Fermi surface indicate the feature of semiconductor with three elements in the states of Cr^{3+} , S^{2-} and Se^{2-} , respectively. As compared with pristine CrSSe, the distribution of DOS intensity near E_f for Cr in LiCrSSe is barely changed, which means that participation of Cr ions in charge compensation is limited. While states of S and Se are obviously getting filled by electrons during lithium intercalation, refer to processes of reduction in line with the results of XAS. Apart from this, partial density of states (PDOSs) of S-3p and Se-4p for CrSSe and LiCrSSe demonstrate similar charge distributions for various positions of atoms without discrepancies in Figure S9, which is a clarification of the uniformity of redox reactions for atoms of S and Se.

Fabrication of full batteries with CrSSe cathode enabled by Li_3N film

Concern for safety hazard of the lithium metal anode, soft carbon is chosen as the alternative in fabrication of the full cell to pair with CrSSe, in which a strategy has to be proposed to meet the requirement of battery for lithium ions. As far as we know, Li_3N is considered to be an effective Li^+ donor with a thermodynamic potential of degradation as low as 0.44 V.²⁹ Thus, Li_3N film was prepared directly on the surface of electrode, which was done by depositing metal lithium and reacting with nitrogen gas instantly within the thermal evaporation device, serving as the prelithiation material in the battery. As no lithium containing for CrSSe and soft carbon, both can be prelithiated to configurate full batteries, respectively.

After 4 μm lithium film being deposited and nitridated upon CrSSe (named as CrSSe- Li_3N), the appearance of electrode turns to wholly dusty blue (Figure S10) and newly-formed grains can be clearly seen on the surface under SEM. Energy dispersive spectrum (EDS) mappings also display the sparser distributions of Cr, S, Se as well as a denser distribution of N (Figure 4a), implying the presence of nitride coating. The XRD measurement of the CrSSe- Li_3N was then performed in Figure 4b. The Bragg reflections of 22.9° and 28.3° are the clear evidence of the existence of $\alpha\text{-Li}_3\text{N}$. In addition, intensities of peaks at 15.2° , 30.9° and 35.2° for CrSSe have weakened with the (003) peak of LiCrSSe at 14.4° and peak at 26.5° denoted as Li_2S or Li_2Se appeared, which means that insertion and even part of conversion reactions have happened upon lithium deposition at the surface of electrode, though the inner remains to be CrSSe. In the first charge of the CrSSe- Li_3N in half-cell (Figure 4c), short plateau voltages of 1.70 and 2.25 V indicate the oxidation of $\text{Li}_2\text{S}/\text{Li}_2\text{Se}$ and the long plateau at 2.75 V indicates the deintercalation process with the XRD pattern of recharged cathode being recognized as the oxidized

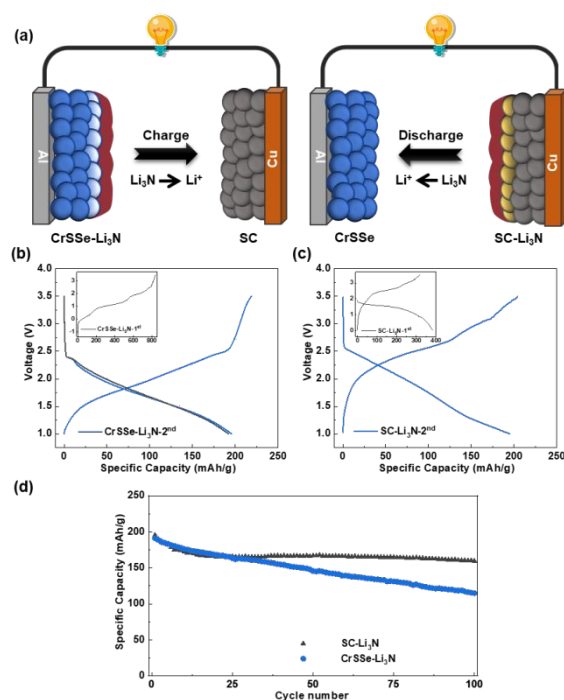


Figure 5. (a) Schematic illustrations for new types of full batteries; charge/discharge curves of (b) CrSSe- Li_3N /SC and (c) CrSSe/SC- Li_3N full-cells; (d) cycling performance at 0.5C.

state of product. Therefore, it can be concluded that CrSSe which has been chemically lithiated can be reversed electrochemically. However, as comparing the charge/discharge curve of the second cycle with the half-cell of CrSSe, though the specific capacity has no big changed, the sloped region of voltage obviously gets bigger while the platform gets shorter also with a faster capacity decay (Figure S11), which related to the nanosized electrode after the happening of initial conversion reaction.^{5, 30}

As the same thickness of Li_3N film was formed on soft carbon (named as SC- Li_3N) with similar morphology of grains at the surface (Figure 4d), things are much easier for there is no need to worry the structure degradation of electrode material. In the half-cell of SC- Li_3N in Figure 4e, the initial charge curve presents a long plateau at 1.08 V, which is exactly the decomposition potential of Li_3N . Since the second cycle, it performs just like the half-cell of untreated soft carbon yet with a better cycling stability (Figure S12), probably because the Li_3N residue left on the electrode acting as the artificial SEI layer and making the interface more stable.³¹

Two types of full cells, that is, CrSSe- Li_3N /SC and CrSSe/SC- Li_3N , were constructed subsequently, whose illustrations are depicted in Figure 5a. The prelithiation processes of two cells are quite different, for the battery of CrSSe- Li_3N /SC charge while that of CrSSe/SC- Li_3N discharge at first. In this case, it is reasonable that the first charge capacity of CrSSe- Li_3N /SC is much lower than that of CrSSe/SC- Li_3N full-cell because more

residue of lithium left on the surface of soft carbon to form the solid electrolyte interface after the initial discharge process of CrSSe-Li₃N/SC. Whereafter, both two cells can operate reversibly and achieve the 2nd discharge capacity of ~195 mAh g⁻¹ within 3.5-1.0 V (Figure 5b, c). As to the cycle performance, obvious discrepancy can be seen after cycling 30 times. What's more, 81.7% of the initial capacity left after 100 cycles for CrSSe/SC-Li₃N while only 60.1% left for CrSSe-Li₃N/SC, as the result of influences on electrode during the synthesis of Li₃N film (Figure 5d). Anyhow, both two cells can be smoothly operating, indicating our successful design of this kind of full battery especially for the lithium-free cathode.

Experimental

Sample preparation

CrSSe was prepared by oxidation of NaCrSSe with iodine and NaCrSSe can be obtained by the simple combination of elements, which is a method originated by the synthesis of VS₂ from LiVS₂,³² in accordance with the equation expressed as $2\text{NaCrSSe} + \text{I}_2 = \text{CrSSe} + 2\text{NaI}$ (1)

The reaction occurs within the environment of acetonitrile to make certain the depletion of iodine can be clearly checked by the variation of solution color without the disturbance by starch complexes. In a typical reaction, NaCrSSe was placed in absolute acetonitrile with stirring firstly and treated with I₂ solution drop by drop in Ar atmosphere. After the solution becomes colorless, stirring was continued overnight. Then the product of CrSSe should be filtered and washed with absolute acetonitrile, finally dried in vacuum at 60 °C.

Electrochemical measurement

In terms of the preparation of CrSSe cathode, active materials, carbon black and poly(vinylidene difluoride) (PVDF) were mixed with a weight ratio of 8: 1: 1, stirred in N-methyl-2-pyrrolidone (NMP) for 8 hours, then uniformly coated on the aluminum foil. It was dried within the oven of vacuum at 60 °C before cut into round electrodes (diameter =12 mm) with ~1 mg of CrSSe contained for each. The anode of soft carbon can be made just like the above procedures containing ~1.2 mg active materials for each. The electrolyte was made up of 1M lithium bis(trifluoromethanesulfonyl) imide dissolved in 1:1 volume 1,3-dioxolane (DOL) and 1,2-dimethoxyethane (DME) with 1 wt. % LiNO₃. Coin cells of 2032-type were assembled for all the electrochemical tests, in which the galvanostatic cycling was carried out on Neware battery testers and cyclic voltammetry measurements were investigated by Zahner system.

Characterizations

Cr and Se K-edge XAS was measured at beamline 7-BM (QAS) of National Synchrotron Light Source II (NSLS-II) in Brookhaven National Laboratory (BNL). The data were collected in the transmission mode. The reference spectrum of Cr metal foil or

Se were simultaneously collect during each measurement and used for energy calibration. S K-edge XAS spectra were obtained in the fluorescence mode at beamline 4B7A in Beijing Synchrotron Radiation Facility and beamline 9-BM of Advanced Photon Source (APS) at Argonne National Laboratory (ANL). The X-ray absorption near-edge structure (XANES) and Extended X-ray absorption fine structure (EXAFS) spectra were processed using the Athena software package.³³ Other data are recorded in Tianmu Lake Institute of Advanced Energy Storage Technologies (TIES) by X-ray Diffraction (Bruker D8 Advance), scanning electron microscope (Hitachi Regulus 8100), scanning transmission electron microscopy (JEOL ARM200F, 200 keV), Raman (Renishaw, INVIA REFLEX), X-ray photoelectron spectroscopy (PHI-5000 Versa Probe III), respectively.

Noted that all the above operations were employed within the argon-filled glove box or the room of dry air, as NaCrSSe, CrSSe and Li₃N are all sensitive to the moist air.

DFT+U calculations

The DFT calculations in the work were carried out based on the projector-augmented wave (PAW) method using DFT theory,³⁴ executed with the VASP program.³⁵ The Perdew-Burke-Ernzerhof functional was used for exchange correlation.³⁶ Spin polarization was enabled. The CINEB calculation was carried out for searching the minimum-energy path.³⁷ The effective U_{eff} value was set to 3.5 eV for Cr as discussed in electronic structure calculations on NaCrS₂.^{21, 22} The plane wave cutoff energy was set to 550 eV and 3 × 3 × 1 Monkhorst-Pack k-point mesh was set for Li_xCrSSe 2 × 2 × 1 supercells. The convergence criterion is to confirm the total energy converged to 2 meV per atom.

Conclusions

In summary, a novel transition metal dichalcogenides (TMDs) CrSSe has been successfully devised and explored, for which more than one complete lithium can be steadily (de)intercalating, producing a capacity of 190 mAh g⁻¹ between 3.5-1.0 V, all contributed by the anionic redox of S and Se. Besides, the impressive capacity retention of 81.5% for 1000 cycles at 20C and the awesome capacity of 101.7 mAh g⁻¹ at 200C, all presenting high-rate properties of CrSSe. Remarkably, novel full battery configurations of CrSSe/Li₃N/electrolyte/C and CrSSe/electrolyte/Li₃N/C are fabricated, in which Li₃N film was in-situ generated on the surface of electrode as the lithium source, avoiding the safety problem of lithium metal batteries and promoting the application of lithium-free cathodes. Moreover, it has been disclosed that usage of Li₃N film on anode for prelithiation is more proper than on cathode with a superior cycle performance. All in all, creating of CrSSe is an excellent supplement to the system of TMDs with durability, rate capability, especially the dual anionic reaction which has never been seen before, offering valuable clues for the design of other

layered materials. Aside from this, invention of the groundbreaking full battery makes these lithium-free cathodes be taken advantage of without the necessary consideration of metallic lithium anode, which should be the trend being well accepted and moved forward in the near future.

Conflicts of interest

There are no conflicts to declare.

Acknowledgements

This work was financially supported by the NSAF (Grant No. 19 21773037), the National Key Scientific Research Project (Grant No. 2016YFB090150) and Tianmu Lake Institute of Advanced Energy Storage Technologies Scientist Studio Program [No. TIES-SS0002]. The work done at Brookhaven National Laboratory was supported by the Assistant Secretary for Energy Efficiency and Renewable Energy, Vehicle Technology Office of the United States through the Advanced Battery Materials Research Program (BMR) under Contract DE-SC0012704. This research used resources at beamline 7-BM (QAS) of the National Synchrotron Light Source II, a U.S. Department of Energy (DOE) Office of Science User Facility operated for the DOE Office of Science by Brookhaven National Laboratory under Contract No. DE-SC0012704. Research conducted at beamline 9-BM used resources of the Advanced Photon Source, an Office of Science User Facility operated for the US DOE by Argonne National Laboratory under Contract No. DE-AC02-06CH11357. In addition, the authors gratefully thank Shanghai Key Laboratory of Molecular Catalysts and Innovative Materials, Department of Chemistry & Laser Chemistry Institute, Fudan University.

Notes and references

- B. Rao, R. Francis and H. Christopher, *J Electrochem Soc*, 1977, **124**, 1490.
- United States Pat.*, US 4224390, 1980.
- M. S. J. C. r. Whittingham, *Chem Rev*, 2004, **104**, 4271-4302.
- E. A. Suslov, O. V. Bushkova, E. A. Sherstobitova, O. G. Reznitskikh and A. N. Titov, *Ionics*, 2015, **22**, 503-514.
- J. E. Trevey, C. R. Stoldt and S.-H. Lee, *J Electrochem Soc*, 2011, **158**.
- W. Fang, H. Zhao, Y. Xie, J. Fang, J. Xu and Z. Chen, *Acs Appl Mater Inter*, 2015, **7**, 13044-13052.
- L. Zhang, D. Sun, Q. Wei, H. Ju, J. Feng, J. Zhu, L. Mai, E. J. Cairns and J. Guo, *Journal of Physics D: Applied Physics*, 2018, **51**.
- D. Murphy, F. Di Salvo and J. J. J. o. S. S. C. Carides, *Journal of Solid State Chemistry*, 1979, **29**, 339-343.
- J. B. Goodenough and Y. Kim, *Journal of Solid State Chemistry*, 2009, **182**, 2904-2911.
- C. Van Bruggen, R. Haange, G. Wiegers and D. J. P. B. c. De Boer, *Physica B+c*, 1980, **99**, 166-172.
- S. Kobayashi, H. Ueda, D. Nishio-Hamane, C. Michioka and K. Yoshimura, *Phys Rev B*, 2014, **89**.
- L. Liang, X. Sun, D. K. Denis, J. Zhang, L. Hou, Y. Liu and C. Yuan, *ACS Appl Mater Interfaces*, 2019, **11**, 4037-4046.
- H. Martinez, A. Benayad, D. Gonbeau, P. Vinatier, B. Pecquenard and A. Levasseur, *Applied Surface Science*, 2004, **236**, 377-386.
- B. Ma, Z. Nie, C. Liu, M. Kang, F. Bardelli, F. Chen and L. Charlet, *Science China Chemistry*, 2014, **57**, 1300-1309.
- Y. Duan, B. Zhang, J. Zheng, J. Hu, J. Wen, D. J. Miller, P. Yan, T. Liu, H. Guo, W. Li, X. Song, Z. Zhuo, C. Liu, H. Tang, R. Tan, Z. Chen, Y. Ren, Y. Lin, W. Yang, C. M. Wang, L. W. Wang, J. Lu, K. Amine and F. Pan, *Nano Lett*, 2017, **17**, 6018-6026.
- K. Feng, F. Wang, X. Yang, H. Zhang, X. Li and H. Zhang, *J Mater Chem A*, 2019, **7**, 567-573.
- W. K. Pang, J. Y. Lee, Y. S. Wei and S. H. Wu, *Mater Chem Phys*, 2013, **139**, 241-246.
- K. B. Ma X, Ceder G., *J Electrochem Soc*, 2010, **157(8)**, A925.
- V. Werth, K. Volgmann, M. M. Islam, P. Heitjans and T. Bredow, *Zeitschrift für Physikalische Chemie*, 2017, **231**.
- I. Arcon, B. Mirtic and A. J. J. o. t. A. C. S. Kodre, *Journal of the American Ceramic Society* 1998, **81**, 222-224.
- T. Wang, G. X. Ren, Z. Shadike, J. L. Yue, M. H. Cao, J. N. Zhang, M. W. Chen, X. Q. Yang, S. M. Bak, P. Northrup, P. Liu, X. S. Liu and Z. W. Fu, *Nat Commun*, 2019, **10**, 4458.
- Z. Shadike, Y. N. Zhou, L. L. Chen, Q. Wu, J. L. Yue, N. Zhang, X. Q. Yang, L. Gu, X. S. Liu, S. Q. Shi and Z. W. Fu, *Nat Commun*, 2017, **8**, 566.
- S. Saha, G. Assat, M. T. Sougrati, D. Foix, H. Li, J. Vergnet, S. Turi, Y. Ha, W. Yang, J. Cabana, G. Rousse, A. M. Abakumov and J.-M. Tarascon, *Nature Energy*, 2019, **4**, 977-987.
- D. W. J. P. R. B. Fischer, *Phys Rev B*, 1973, **8**, 3576.
- B. Joseph, A. Iadecola, L. Simonelli, Y. Mizuguchi, Y. Takano, T. Mizokawa and N. L. Saini, *J Phys Condens Matter*, 2010, **22**, 485702.
- N. L. Saini, T. Mizokawa, E. Magnano, S. Nappini, F. Bondino, H. Takeya, Y. Mizuguchi, Y. Takano and K. B. Garg, *Phys Rev B*, 2014, **90**.
- S. Chattopadhyay and A. J. J. o. t. P. S. o. J. P. Deshpande, *Journal of the Physical Society of Japan*, 1986, **55**, 2320-2325.
- R. Friend, D. Jerome, W. Liang, C. Mikkelsen and A. J. J. o. P. C. S. S. P. Yoffe, *Journal of Physics C: Solid State Physics*, 1977, **10**, L705.
- A. J. S. S. I. Rabenau, *Solid State Ionics*, 1982, **6**, 277-293.
- P. Gibot, M. Casas-Cabanas, L. Laffont, S. Levasseur, P. Carlach, S. Hamelet, J. M. Tarascon and C. Masquelier, *Nat Mater*, 2008, **7**, 741-747.
- K. Park and J. B. Goodenough, *Adv Energy Mater*, 2017, **7**.
- D. W. Murphy, C. Cros, F. J. Di Salvo and J. J. I. C. Waszczak, *Inorg Chem Commun*, 1977, **16**, 3027-3031.
- B. Ravel and M. Newville, *J Synchrotron Radiat*, 2005, **12**, 537-541.
- P. E. Blöchl, *Phys Rev B*, 1994, **50**, 17953-17979.
- G. Kresse and J. Furthmüller, *Phys Rev B*, 1996, **54**, 11169-11186.
- J. P. Perdew, K. Burke and M. Ernzerhof, *Phys Rev Lett*, 1996, **77**, 3865-3868.
- G. Henkelman, B. P. Uberuaga and H. Jónsson, *The Journal of Chemical Physics*, 2000, **113**, 9901-9904.

